Published in final edited form as:
Biol Psychiatry. 2015 February 1; 77(3): 276–284. doi:10.1016/j.biopsych.2014.02.014.

Ventromedial prefrontal cortex is critical for the regulation of amygdala activity in humans

Julian C. Motzkin[1,2,3], **Carissa L. Philippi**[1], **Richard C. Wolf**[1,2], **Mustafa K. Baskaya**[4], and **Michael Koenigs**[1,*]

[1]Department of Psychiatry, University of Wisconsin-Madison, 6001 Research Park Blvd., Madison, Wisconsin, 53719, USA

[2]Neuroscience Training Program, University of Wisconsin-Madison, 1300 University Ave., Madison, Wisconsin, 53706, USA

[3]Medical Scientist Training Program, University of Wisconsin-Madison, 750 Highland Ave., Madison, Wisconsin, 53705, USA

[4]Department of Neurological Surgery, University of Wisconsin-Madison, 600 Highland Ave., Madison, Wisconsin, 53792, USA

Abstract

Background—Dysfunction in ventromedial prefrontal cortex (vmPFC) is believed to play a pivotal role in the pathogenesis of mood and anxiety disorders. Leading neurocircuitry models of these disorders propose that hypoactivity in vmPFC engenders disinhibited amygdala activity, and consequently, pathologically elevated levels of negative affect. This model predicts that a selective loss or diminution of vmPFC function would result in heightened amygdala activity. While this prediction has been borne out in rodent lesion and electrophysiological studies using fear conditioning and extinction paradigms, there has not yet been a definitive test of this prediction in humans.

Methods—In this study, we tested this prediction through a novel use of fMRI in n=4 neurosurgical patients with focal, bilateral vmPFC damage.

Results—Relative to neurologically healthy comparison subjects, the vmPFC lesion patients exhibited potentiated amygdala responses to aversive images as well as elevated rest-state amygdala functional connectivity. We observed no comparable group differences for activity in other brain regions.

*Author for correspondence: mrkoenigs@wisc.edu, 608-263-1679 (phone), 608-263-9340 (fax).

FINANCIAL DISCLOSURES

The authors report no biomedical financial interests or potential conflicts of interest.

Conclusions—These results provide unique evidence for the critical role of vmPFC in regulating amygdala activity in humans, and help elucidate the causal neural interactions that underlie mental illness.

Keywords

Prefrontal Cortex; Amygdala; Emotion; Lesion; fMRI; Anxiety

INTRODUCTION

The ventromedial prefrontal cortex (vmPFC) is a key neural substrate of human social and affective function (1-3), and is considered central to the pathophysiology of mood and anxiety disorders (4, 5). However, the precise mechanisms by which vmPFC contributes to affective processing are not fully understood. The predominant neural circuitry model proposes that vmPFC serves to regulate negative affect via top-down inhibition of brain regions involved in processing negative emotion—particularly the amygdala—and that pathologically elevated levels of negative affect in mood and anxiety disorders result from deficient vmPFC-mediated inhibition of amygdala activity (6-8). Multiple lines of convergent evidence support this inhibitory model of vmPFC function. In rodents, infralimbic cortex (the purported homolog of human vmPFC) has been shown to mediate sustained extinction of conditioned fear through inhibition of the amygdala (7, 9, 10). In humans, functional imaging studies have demonstrated that activity in vmPFC and amygdala is inversely related during the extinction of conditioned fear (11) and during the volitional suppression of negative emotion (12-14), with the inverse coupling between vmPFC and amygdala commonly disrupted in mood and anxiety disorders (6, 7, 13). Anatomical tracing studies in rodents and non-human primates have identified direct projections from vmPFC to inhibitory interneurons within the amygdala, indicating a viable anatomical substrate for the observed functional relationship (15, 16).

Although these findings are consistent with the proposal that vmPFC plays a critical and causal role in regulating amygdala activity, human vmPFC lesions are commonly associated with changes in personality and behavior (e.g., social disinhibition, blunted affect) that are notably distinct from those typical of anxious and depressive psychopathology (17, 18). Further, focal vmPFC damage has been shown to *reduce* the likelihood of developing PTSD and depression (19, 20), consistent with previous studies indicating that metabolism in the subgenual cingulate region of vmPFC is increased (not decreased) in depression (21). Thus, it remains unknown whether the disruption of vmPFC function would in fact significantly disinhibit amygdala activity in humans. In the present study, we addressed this empirical gap through a novel application of fMRI to neurological patients with focal, bilateral vmPFC lesions. Using this unique approach, we show that vmPFC exerts a causal influence on amygdala activity in humans.

METHODS

Participants

The target lesion group consisted of four adult neurosurgical patients with extensive bilateral parenchymal damage, largely confined to the vmPFC—defined as the medial one-third of the orbital surface and the ventral one-third of the medial surface of prefrontal cortex, bilaterally (Fig. 1). Each of the four patients underwent surgical resection of a large anterior cranial fossa meningioma via craniotomy. Initial clinical presentations included subtle or obvious personality changes over several months preceding surgery. On post-surgical MRI, although vasogenic edema largely resolved, there were persistent T_2-weighted signal changes, consistent with gliosis, in the vmPFC bilaterally. All experimental procedures were conducted more than three months after surgery, when the expected recovery was complete. At the time of testing, all patients had focal, stable MRI signal changes and resection cavities and were free of dementia and substance abuse.

Nineteen healthy adults with no history of brain injury, neurological or psychiatric illness, or current use of psychoactive medication were recruited as a normal comparison (NC) group. From the full NC group, we selected a subsample of n=10 subjects who were more closely matched to the vmPFC patients in age and gender, to corroborate results from the larger NC sample. Demographic and neuropsychological data for the vmPFC and NC groups are summarized in Table 1.

We assessed amygdala function in two separate fMRI experiments: an event-related task involving the presentation of aversive and neutral pictures and a rest-state scan in which subjects passively viewed a fixation cross.

Event-related fMRI task

During the fMRI task, adapted from a previous paradigm shown to elicit strong amygdala activation in healthy subjects (22), subjects viewed 64 unique images drawn from the International Affective Picture System (IAPS) (23), divided evenly among pictures with aversive and neutral content (see Fig. S1 **and** Table S1 for details). Aversive stimuli consisted of 32 negative/unpleasant and arousing images, based on published norms (23, 24) (Valence: 2.01±0.39; Arousal: 6.25±0.7). Neutral stimuli consisted of 32 images with neutral valence and low arousal ratings (Valence: 4.96±0.21; Arousal: 2.95±0.77). All images were preceded by one of three visual cues (“X”, “O”, or “?”). The “X” and “O” cues indicated that the subsequent image would be aversive or neutral, respectively, whereas the “?” cue provided no information regarding the emotional content of the image (equal likelihood of aversive or neutral content). Each experimental trial consisted of a cue presented for 2 s, followed—after a jittered inter-stimulus interval (ISI) (range: 2-8 s)—by a 1 s picture presentation. After a second jittered ISI (range: 5-9 s), subjects had 4 s to rate their emotional response to the image using a 4-item scale ranging from 1 (“very positive”) to 4 (“very negative”) (see Table S2 for rating data). Prior to scanning, subjects were informed of all cue-picture contingencies and completed a practice task consisting of 16 unique trials (4 per cue-picture pair) to ensure task comprehension.

MRI data acquisition

All structural and functional MRI data were acquired using a 3.0 T GE Discovery MR750 scanner equipped with an 8-channel radio-frequency head coil array (General Electric Medical Systems; Waukesha, WI). High-resolution T_1-weighted anatomical images were acquired using an inversion-recovery spoiled GRASS [SPGR] sequence (TR=8.2ms, TE=3.2ms, α=12°, FOV=256×256mm, matrix=256×256, in-plane resolution=1×1mm^2, slice thickness=1mm, 1024 axial slices). To facilitate lesion segmentation, we collected a separate T_2-weighted FLAIR scan (TR=8650ms, TE=136ms, α=0°, FOV=220×220mm^2, matrix=512×512, in-plane resolution=0.43×0.43mm^2, slice thickness=5 mm, gap 1mm, 25 axial slices).

Baseline resting cerebral blood flow (CBF) was estimated using a 3D fast spin echo spiral sequence with pseudocontinuous arterial spin labeling (pcASL) (25-27) and background suppression for quantitative perfusion measurements (TR=4653ms, TE=10.5ms, post-labeling delay=1525ms, labeling duration=1450ms, eight interleaved spiral arms with 512 samples at 62.5-kHz bandwidth and 38 4-mm thick slices, number of excitations=3, scan duration=4.5min).

Whole-brain functional scans (task and rest) were acquired using a T_2*-weighted gradient-echo echoplanar imaging (EPI) sequence (TR=2000ms; TE=22ms; α=79; FOV=224×224mm^2; matrix=64×64, in-plane resolution=3.5×3.5mm^2, slice thickness=3mm, gap=0.5mm, 38° interleaved axial oblique slices). Field maps were acquired using two separate acquisitions (TR=600ms, TE_1=7ms, TE_2=10ms, α=60°, FOV=240×240mm, matrix=256×128, slice thickness=4mm, 33 axial oblique slices). Rest-state functional images were collected while subjects lay still and awake, passively viewing a fixation cross for 5 minutes. The two task runs lasted 12.4 minutes each. Scans were acquired in the following order: pcASL, field map, rest, task, T1, T2-FLAIR.

Heart rate data acquisition

Cardiac data were acquired at 100 Hz with GE's photoplethysmograph, affixed to the left index finger throughout the scan session. Heart rate data were available for n=12 NC subjects and all n=4 vmPFC lesion patients.

Lesion segmentation and image normalization

Individual vmPFC lesions were visually identified and manually segmented on the T_1-weighted images. Lesion boundaries were drawn to include areas with gross tissue damage or abnormal signal characteristics on T_1 or T_2 FLAIR images. T_1-weighted images were skull-stripped, rigidly co-registered with a functional volume from each subject, then diffeomorphically aligned to the Montreal Neurological Institute (MNI) coordinate system using a Symmetric Normalization (SyN) algorithm (28) with constrained cost-function masking to prevent warping of tissue within the lesion mask (29). We created the lesion overlap map (Fig. 1) by computing the sum of aligned binary lesion masks for all four vmPFC patients.

fMRI task preprocessing and analysis

Data analysis was conducted using AFNI (30) and FSL (http://www.fmirb.ox.ac.uk/fsl) software. Individual task runs were slice time corrected, field map corrected (31), motion corrected, smoothed with a 6-mm full-width half-maximum (FWHM) Gaussian kernel, and scaled to percent signal change. Preprocessed task data were concatenated and analyzed using a general linear model (GLM) with separate regressors for each cue and picture type, the rating period, and several regressors of no interest, including six motion covariates from rigid-body alignment (32) and a fourth-order polynomial to model baseline and slow signal drift. Blood oxygen level-dependent (BOLD) signal was modeled by convolving each event with AFNI's default canonical hemodynamic response function (HRF; gamma function). Because the identity of the cue did not significantly alter amygdala responses to the aversive pictures in either group (Table S3), analyses were limited to aversive and neutral stimuli, irrespective of cue. To avoid potential confounds introduced by subject motion, volumes in which more than 10% of voxels were time series outliers were censored prior to conducting the GLM; there were no group differences in the average proportion of censored volumes (χ^2=2.09, P=0.15), or in mean framewise displacement (NC: 0.06±0.06mm, vmPFC: 0.04±0.02mm; W=28, P=0.44). Resulting whole-brain maps of voxelwise β-values for aversive and neutral pictures were aligned to MNI space and resampled to 3mm^3 isotropic resolution for second-level analyses.

To identify brain regions responsive to aversive stimuli, we performed a whole-brain, two-tailed paired-sample t-test between responses to aversive and neutral pictures in the full NC group. Resulting statistical maps were family-wise error (FWE) corrected for multiple comparisons across the whole brain at the cluster level (P_{FWE}<0.05), using a height threshold of P<0.001 (33, 34). A corrected P_{FWE}<0.05 was achieved using a cluster extent threshold of 38 voxels (1026mm^3), calculated using Monte Carlo simulations with 3dClustSim in AFNI. Significant clusters from the aversive>neutral contrast (10 total) were used as functional regions of interest (ROIs) for subsequent between-groups analyses.

To visualize group-averaged BOLD responses to pictures within individual ROIs, we conducted a second GLM, replacing the canonical HRF with a series of nine TENT functions in order to deconvolve the raw BOLD signal. This model yielded β-values for each of 9 TRs from 0-16 seconds after picture onset. Because functional ROIs were derived using the canonical HRF, estimated response data from the deconvolution model were used for display only.

In light of the small sample size of vmPFC lesion patients, we used non-parametric Mann-Whitney-Wilcoxon tests to evaluate our main *a priori* hypothesis regarding amygdala activity. Specifically, we focused our between-groups analyses on percent signal change estimates extracted from functionally-derived right and left amygdala ROIs (amygdala clusters from the aversive>neutral contrast in the NC group). We used functional ROIs to ensure that group comparisons were conducted within functionally homogenous regions within the amygdala (i.e., regions that respond strongly to aversive relative to neutral stimuli) (35). However, to confirm that group comparisons within functionally-derived amygdala ROIs reflected differences in amygdala activity *per se*, we conducted additional

between-groups tests using values extracted from atlas-defined anatomical ROIs in the right and left amygdala, created using the Talairach daemon in AFNI. To examine subregions of the amygdala, we conducted follow-up analyses using hand-drawn, atlas-defined ROIs in the central nucleus of the amygdala (CeA) (36).

To test the specificity of observed effects to the amygdala, we conducted follow-up analyses on percent signal change values extracted from the eight remaining functionally-derived non-amygdala comparison ROIs (e.g., bilateral visual cortex, lateral temporal cortex, thalamus, etc.), in which we predicted normal responses to pictures for the vmPFC patients. All group comparisons were corroborated with the subsample of n=10 age- and gender-matched NC subjects in order to verify that group effects were not driven by potential differences in demographic variables. All tests were considered significant at $P<0.05$.

Rest-state functional connectivity analysis

Rest-state scans were preprocessed as in the task analysis, with de-spiking and band-pass filtering ($0.01<f<0.1$) conducted prior to smoothing. Two NC subjects were excluded from the rest-state analysis (n=1 with excessive head motion (>2mm) (37), n=1 due to errors in field map correction) for a total sample size of n=17 NC subjects. Functional connectivity was assessed using task-derived left and right amygdala ROIs, masked by the anatomical amygdala ROI to exclude voxels outside the amygdala and aligned to native space, and confirmed using independent anatomically-defined CeA ROIs. Functional connectivity was computed using a GLM with the mean resting-state BOLD time series extracted from each subject-specific ROI and nine regressors of no interest, including six motion covariates, average time series from white matter and ventricles, and a second-order polynomial to model baseline signal and slow drift. To further control for subject motion, volumes in which more than 10% of voxels were time series outliers were censored in the GLM. Correlation coefficients were converted to z-scores via Fisher's r-to-z transform and corrected for degrees of freedom. Resulting z-score maps were aligned to MNI space and resampled to $3mm^3$ isotropic resolution for subsequent second-level analyses.

Because we had no *a priori* hypothesis regarding the particular brain regions where vmPFC damage would yield altered amygdala connectivity, we conducted an exploratory whole-brain voxelwise non-parametric comparison between amygdala connectivity maps in the NC and vmPFC groups. Resulting statistical maps were FWE-corrected for multiple comparisons across the whole brain at the cluster level ($P_{FWE}<0.05$), using a height threshold of $P<0.005$ (33, 34). A corrected $P_{FWE}<0.05$ was achieved using a cluster extent threshold of 90 voxels (2430 mm^3), calculated using Monte Carlo simulations.

Cerebral perfusion analysis

Quantitative CBF images from pcASL were rigidly co-registered with a T_2*-weighted EPI volume from the task scan and normalized to MNI space. Normalized CBF volumes were scaled to whole-brain CBF (after masking out the lesion in vmPFC patients) and smoothed with a 6mm FWHM Gaussian kernel. To rule out differences in baseline cerebral perfusion, we examined group differences in mean whole-brain CBF, as well as differences in scaled CBF for all ROIs using non-parametric Mann-Whitney-Wilcoxon tests.

Heart rate analysis

To assess cardiac responses to picture stimuli, we computed trial-wise estimates of heart rate change for each subject, as previously described (38). Cardiac R-spikes were identified using interactive beat detection software. Trials with ectopic beats, missed beats, or periods of noisy signal (where beat detection failed), were excluded from further analysis (NC group: n=2 with one excluded trial, n=1 with two excluded trials, n=2 with three excluded trials; vmPFC group: n=1 with two excluded trials). R-R intervals were transformed into heart rate in beats per minute, in 500 ms bins. Changes in heart rate were determined by subtracting the mean heart rate for 1 s preceding each picture from the heart rate at each 500 ms after picture onset. As in previous studies, the maximum cardiac deceleration (i.e., heart rate decrease) during the first 3 s of picture viewing was used as an index of the physiological response to each picture (38). Group differences in cardiac deceleration were computed separately for aversive and neutral pictures using non-parametric Mann-Whitney-Wilcoxon tests.

RESULTS

fMRI task

During the fMRI task, both groups rated aversive pictures as significantly more negative than the neutral pictures, with no differences between groups in ratings for either emotion category (Table S2). Relative to neutral pictures, aversive pictures elicited robust bilateral amygdala activation in both the NC subjects (Fig. 2a and Table 2) and vmPFC lesion patients (Fig. 2b). To examine group differences in amygdala activity, we extracted percent signal change estimates from functionally-derived right and left amygdala ROIs—clusters of supra-threshold amygdala voxels from the aversive>neutral contrast in the NC group (Fig. 3a). In support of our main hypothesis, vmPFC lesion patients exhibited significantly greater right amygdala activation to aversive pictures than did NC subjects (W=6, P=0.006; Fig. 3b**,** Table 3). We observed similar group differences in activation to aversive pictures using an anatomically-defined right amygdala ROI (W=13, P=0.04) as well as an anatomically-defined right CeA ROI (W=13, P=0.04). This central finding was corroborated in a smaller sample of ten NC subjects closely matched in age and gender to the vmPFC group (W=2, P=0.008; Table S4), suggesting that the findings were not driven by group differences in demographic factors. No significant group differences were observed in any left amygdala ROI (Functional ROI: W=28, P=0.46; Anatomical ROI: W=24, P=0.29; CeA ROI: W=24, P=0.29; Fig 3**,** Table 3, Table S4**)**.

To test the specificity of group differences to the amygdala, we conducted follow-up analyses in the eight remaining functionally-derived ROIs from the aversive>neutral picture contrast (e.g. visual cortex, lateral temporal cortex, thalamus, etc.) and found no consistent group differences in the response to aversive or neutral pictures in the non-amygdala comparison ROIs (Tables 3 and S4). To ensure that group differences in the amygdala were not due to baseline differences in amygdala perfusion following vmPFC damage, we estimated CBF using pcASL prior to both functional scans in all subjects. There were no significant differences between the NC and vmPFC groups in whole brain CBF, nor were there differences in relative CBF for any ROI used in group comparisons, including right

amygdala (Tables S5 and S6). Finally, it is unlikely that the observed findings are due to systematic group differences in the shape of the hemodynamic response, since there were no apparent differences in the estimated hemodynamic response in motor cortex to button press (Fig. S2) or in visual and temporal comparison ROIs in response to aversive pictures (Fig. S3).

Heart rate response to pictures

To determine whether group differences in amygdala activity were accompanied by comparable differences in peripheral physiological responses, we investigated stimulus-evoked reductions in heart rate in response to the picture stimuli. Consistent with previous studies using the same stimuli, both groups exhibited cardiac deceleration in response to aversive and neutral pictures (38, 39). However, contrary to the amygdala fMRI results, the magnitude of stimulus-evoked cardiac deceleration was significantly *lower* in vmPFC lesion patients than in the NC subjects for aversive pictures (NC: −1.3±0.67; vmPFC: −0.52±0.31; W=6, P=0.03; Fig. S4). We observed similar, though non-significant, reductions in cardiac deceleration in response to neutral pictures (NC: −1.4±0.89; vmPFC: −0.60±0.30; W=11, P=0.13). There was no significant difference between groups in overall mean heart rate across the scan session (NC: 62.7±9; vmPFC: 75.9±12; W=11, P=0.13).

Rest-state functional connectivity

To investigate whether group differences in amygdala activation during the task were also associated with group differences in amygdala rest-state functional connectivity, we conducted a secondary analysis using amygdala seed ROIs. Consistent with the results of the fMRI task, the rest-state functional connectivity analysis revealed greater connectivity between the right amygdala and a region of right anterolateral temporal cortex in vmPFC lesion patients (Fig. 4**,** Fig. S5). This finding was replicated using an independent anatomically-defined CeA ROI (Fig. S6**)**.

DISCUSSION

Through a novel application of fMRI in human lesion patients with bilateral vmPFC damage, we have demonstrated a critical role for vmPFC in regulating amygdala activity. Specifically, we found that vmPFC lesions were associated with increased right amygdala reactivity to aversive stimuli, as well as increased rest-state connectivity with anterior temporal cortex. These findings are directly relevant to neural circuitry models of emotion regulation and affective psychopathology.

One influential model of affective psychopathology proposes two key features: (i) vmPFC dysfunction results in disinhibition of the amygdala and (ii) the resultant amygdala hyperactivity engenders pathologically high levels of anxiety and negative affect (6-8). Although our results unequivocally support feature (i) of this model, they seem to complicate feature (ii), at least as it pertains to human affective processing. Using fear conditioning and extinction paradigms, an elegant set of rodent studies have demonstrated a causal chain between activity in infralimbic cortex (the purported homolog of human vmPFC), inhibition of amygdala, and extinction of conditioned behavioral and physiological

fear responses (7, 9, 10, 40). Human functional imaging studies have provided correlative data consistent with this model (6, 7, 11-14). However, the causal relationships among vmPFC activity, amygdala activity, and negative affect appear to be more complicated in humans. At least two lines of research argue for a more comprehensive model. One line of research involves patients with major depressive disorder (MDD). A number of neuroimaging studies indicate that patients with MDD exhibit abnormally high levels of activity within vmPFC (particularly in the subgenual cortex) (21, 41-44). In addition, MDD patients who are responsive to antidepressant medication or deep brain stimulation tend to exhibit decreased activity in both the subgenual vmPFC and amygdala after treatment (21, 44-46). Furthermore, activity within the subgenual vmPFC has been shown to correlate positively with negative affect in healthy subjects (47-49). The second line of research involves vmPFC lesion patients. It is well established that vmPFC damage results in personality changes more reminiscent of psychopathy (e.g., blunted emotional experience, low emotional expressivity, impulsivity, lack of empathy, reckless decision-making) than anxiety or depression (17, 18, 50). Critically, vmPFC damage has been shown to *reduce* (not increase) the likelihood of developing depression (51) and post-traumatic stress disorder (52). Moreover, vmPFC damage is associated with diminished physiological reactions (e.g., skin conductance responses) to aversive stimuli (53-55). Our heart rate data are consistent with these prior physiological findings. Rather than observing increased cardiac deceleration in response to aversive pictures in the vmPFC lesion patients (as the model might predict based on the amygdala hyperactivity in these patients), we observed *reduced* deceleration in the vmPFC lesion patients relative to the NC subjects. It should be noted, however, that the finding of similar group differences in cardiac deceleration in response to neutral pictures suggests a more general orienting deficit in the vmPFC group. Together, these findings suggest that the role of vmPFC in affective processing is not simply the regulation of negative emotion through inhibition of the amygdala. Rather, vmPFC appears to play a more multifaceted role that could include processes related to self-awareness and self-reflection (56, 57), and/or more direct modulation of emotion-related physiological responses and negative affect.

Anatomical tracing studies in rodents and non-human primates support comparable roles of vmPFC and amygdala in generating emotion-related physiological responses. Amygdala subnuclei (especially CeA) and areas within vmPFC (especially Brodmann areas 24, 25, and 32) send dense, overlapping projections to brainstem and diencephalic nuclei directly involved in coordinating peripheral autonomic changes; namely, lateral hypothalamus, bed nucleus of stria terminalis, parabrachial nucleus, and periaqueductal gray (58-62). Moreover, vmPFC and amygdala are themselves densely and reciprocally interconnected (59). In addition to projections to intercalated interneurons that ultimately inhibit the CeA, the vmPFC shares reciprocal connections with basolateral amygdala, which are thought to be critical for modulating the expression of negative affect (63, 64). Interestingly, we observed similar effects of vmPFC damage on fMRI responses regardless of whether we used a whole amygdala ROI or a CeA ROI (Table 3, Table S4**)**. Further research will be necessary to more clearly delineate the specific contributions of vmPFC and amygdala subregions to human affective function.

Although we did not have any *a priori* hypothesis regarding lateralization, significant group differences in amygdala reactivity to aversive pictures were observed only in the right amygdala (Figure 3, Table 3). Previous meta-analyses offer some support for a functional dissociation of right and left amygdala in rapid, automatic stimulus processing and sustained stimulus evaluation, respectively (65-67). However, the laterality effects observed here may be due to the lesion characteristics of our vmPFC patient sample. Although all lesions involved significant bilateral damage to vmPFC, each patient had slightly greater damage on the right side (Table S7). Future work in larger samples with more heterogeneous vmPFC lesions will be necessary to more conclusively determine the link between lateralization of vmPFC damage and amygdala hyperactivity.

Future studies could also expand the scope of the present findings by using more diverse stimuli and/or task paradigms. One possibility would be to use a fear extinction paradigm, to allow more direct comparisons with rodent data (1, 7). Moreover, previous studies indicate that the amygdala responds to positive valence and may be more sensitive to stimulus arousal than to valence, per se (66-68). To maximize our power to detect group differences in amygdala activation, we limited stimuli to aversive and neutral pictures and used a simple four-item valence rating scale. Future studies could include images with positive valence and more detailed ratings of valence and arousal in order to determine whether changes in amygdala activity following vmPFC damage are specific to negative affect or more broadly related to subjective arousal.

In conclusion, here we demonstrate a critical role for the vmPFC in regulating amygdala activity. Our findings provide unique evidence regarding the causal interactions among brain regions subserving emotion regulation in humans, and offer novel support for the inhibitory influence of vmPFC on amygdala, as proposed in neurocircuitry models of affective dysfunction in mental illness.

Supplementary Material

Refer to Web version on PubMed Central for supplementary material.

ACKNOWLEDGEMENTS

This work was supported by grants from the National Institutes of Health (K01MH086787, T32GM007507, T32GM008692, T32MH018931).

REFERENCES

1. Quirk GJ, Beer JS. Prefrontal involvement in the regulation of emotion: convergence of rat and human studies. Curr Opin Neurobiol. 2006; 16:723–727. [PubMed: 17084617]
2. Fellows LK. Orbitofrontal contributions to value-based decision making: evidence from humans with frontal lobe damage. Ann N Y Acad Sci. 2011; 1239:51–58. [PubMed: 22145875]
3. Damasio AR. The somatic marker hypothesis and the possible functions of the prefrontal cortex. Philos Trans R Soc Lond B Biol Sci. 1996; 351:1413–1420. [PubMed: 8941953]
4. Price JL. Prefrontal cortical networks related to visceral function and mood. Ann N Y Acad Sci. 1999; 877:383–396. [PubMed: 10415660]
5. Myers-Schulz B, Koenigs M. Functional anatomy of ventromedial prefrontal cortex: implications for mood and anxiety disorders. Mol Psychiatry. 2012; 17:132–141. [PubMed: 21788943]

6. Rauch SL, Shin LM, Phelps EA. Neurocircuitry models of posttraumatic stress disorder and extinction: human neuroimaging research--past, present, and future. Biol Psychiatry. 2006; 60:376–382. [PubMed: 16919525]
7. Milad MR, Rauch SL, Pitman RK, Quirk GJ. Fear extinction in rats: implications for human brain imaging and anxiety disorders. Biol Psychol. 2006; 73:61–71. [PubMed: 16476517]
8. Quirk GJ, Gehlert DR. Inhibition of the amygdala: key to pathological states? Ann N Y Acad Sci. 2003; 985:263–272. [PubMed: 12724164]
9. Quirk GJ, Garcia R, Gonzalez-Lima F. Prefrontal mechanisms in extinction of conditioned fear. Biol Psychiatry. 2006; 60:337–343. [PubMed: 16712801]
10. Quirk GJ, Likhtik E, Pelletier JG, Pare D. Stimulation of medial prefrontal cortex decreases the responsiveness of central amygdala output neurons. J Neurosci. 2003; 23:8800–8807. [PubMed: 14507980]
11. Phelps EA, Delgado MR, Nearing KI, LeDoux JE. Extinction learning in humans: role of the amygdala and vmPFC. Neuron. 2004; 43:897–905. [PubMed: 15363399]
12. Urry HL, van Reekum CM, Johnstone T, Kalin NH, Thurow ME, Schaefer HS, et al. Amygdala and ventromedial prefrontal cortex are inversely coupled during regulation of negative affect and predict the diurnal pattern of cortisol secretion among older adults. J Neurosci. 2006; 26:4415–4425. [PubMed: 16624961]
13. Johnstone T, van Reekum CM, Urry HL, Kalin NH, Davidson RJ. Failure to regulate: counterproductive recruitment of top-down prefrontal-subcortical circuitry in major depression. J Neurosci. 2007; 27:8877–8884. [PubMed: 17699669]
14. Delgado MR, Nearing KI, Ledoux JE, Phelps EA. Neural circuitry underlying the regulation of conditioned fear and its relation to extinction. Neuron. 2008; 59:829–838. [PubMed: 18786365]
15. McDonald AJ, Mascagni F, Guo L. Projections of the medial and lateral prefrontal cortices to the amygdala: a Phaseolus vulgaris leucoagglutinin study in the rat. Neuroscience. 1996; 71:55–75. [PubMed: 8834392]
16. Ghashghaei HT, Barbas H. Pathways for emotion: interactions of prefrontal and anterior temporal pathways in the amygdala of the rhesus monkey. Neuroscience. 2002; 115:1261–1279. [PubMed: 12453496]
17. Barrash J, Tranel D, Anderson SW. Acquired personality disturbances associated with bilateral damage to the ventromedial prefrontal region. Dev Neuropsychol. 2000; 18:355–381. [PubMed: 11385830]
18. Eslinger PJ, Damasio AR. Severe disturbance of higher cognition after bilateral frontal lobe ablation: patient EVR. Neurology. 1985; 35:1731–1741. [PubMed: 4069365]
19. Koenigs M, Huey ED, Raymont V, Cheon B, Solomon J, Wassermann EM, et al. Focal brain damage protects against post-traumatic stress disorder in combat veterans. Nat Neurosci. 2008; 11:232–237. [PubMed: 18157125]
20. Koenigs M, Huey ED, Calamia M, Raymont V, Tranel D, Grafman J. Distinct regions of prefrontal cortex mediate resistance and vulnerability to depression. J Neurosci. 2008; 28:12341–12348. [PubMed: 19020027]
21. Mayberg HS, Brannan SK, Tekell JL, Silva JA, Mahurin RK, McGinnis S, et al. Regional metabolic effects of fluoxetine in major depression: serial changes and relationship to clinical response. Biol Psychiatry. 2000; 48:830–843. [PubMed: 11063978]
22. Sarinopoulos I, Grupe DW, Mackiewicz KL, Herrington JD, Lor M, Steege EE, et al. Uncertainty during anticipation modulates neural responses to aversion in human insula and amygdala. Cereb Cortex. 2010; 20:929–940. [PubMed: 19679543]
23. Lang, PJ.; Bradley, MM.; Cuthbert, BN. International affective picture system (IAPS): Affective ratings of pictures and instruction manual. Technical Report A-8. University of Florida; Gainesville, FL: 2008.
24. Ewbank MP, Barnard PJ, Croucher CJ, Ramponi C, Calder AJ. The amygdala response to images with impact. Social cognitive and affective neuroscience. 2009; 4:127–133. [PubMed: 19151376]
25. Okonkwo OC, Xu G, Oh JM, Dowling NM, Carlsson CM, Gallagher CL, et al. Cerebral Blood Flow is Diminished in Asymptomatic Middle-Aged Adults with Maternal History of Alzheimer's Disease. Cerebral cortex. 2012

26. Dai W, Garcia D, de Bazelaire C, Alsop DC. Continuous flow-driven inversion for arterial spin labeling using pulsed radio frequency and gradient fields. Magnetic resonance in medicine: official journal of the Society of Magnetic Resonance in Medicine / Society of Magnetic Resonance in Medicine. 2008; 60:1488–1497.
27. Xu G, Rowley HA, Wu G, Alsop DC, Shankaranarayanan A, Dowling M, et al. Reliability and precision of pseudo-continuous arterial spin labeling perfusion MRI on 3.0 T and comparison with 15O-water PET in elderly subjects at risk for Alzheimer's disease. NMR Biomed. 2010; 23:286–293. [PubMed: 19953503]
28. Avants B, Gee JC. Geodesic estimation for large deformation anatomical shape averaging and interpolation. NeuroImage. 2004; 23(Suppl 1):S139–150. [PubMed: 15501083]
29. Brett M, Leff AP, Rorden C, Ashburner J. Spatial normalization of brain images with focal lesions using cost function masking. NeuroImage. 2001; 14:486–500. [PubMed: 11467921]
30. Cox RW. AFNI: software for analysis and visualization of functional magnetic resonance neuroimages. Comput Biomed Res. 1996; 29:162–173. [PubMed: 8812068]
31. Jezzard P, Clare S. Sources of distortion in functional MRI data. Human Brain Mapping. 1999; 8:80–85. [PubMed: 10524596]
32. Johnstone T, Ores Walsh KS, Greischar LL, Alexander AL, Fox AS, Davidson RJ, et al. Motion correction and the use of motion covariates in multiple-subject fMRI analysis. Hum Brain Mapp. 2006; 27:779–788. [PubMed: 16456818]
33. Carp J. The secret lives of experiments: methods reporting in the fMRI literature. NeuroImage. 2012; 63:289–300. [PubMed: 22796459]
34. Forman SD, Cohen JD, Fitzgerald M, Eddy WF, Mintun MA, Noll DC. Improved Assessment of Significant Activation in Functional Magnetic Resonance Imaging (fMRI): Use of a Cluster-Size Threshold. Magnetic Resonance in Medicine. 1995; 33:636–647. [PubMed: 7596267]
35. Poldrack RA. Region of interest analysis for fMRI. Social cognitive and affective neuroscience. 2007; 2:67–70. [PubMed: 18985121]
36. Oler JA, Birn RM, Patriat R, Fox AS, Shelton SE, Burghy CA, et al. Evidence for coordinated functional activity within the extended amygdala of non-human and human primates. Neuroimage. 2012; 61:1059–1066. [PubMed: 22465841]
37. Power JD, Barnes KA, Snyder AZ, Schlaggar BL, Petersen SE. Spurious but systematic correlations in functional connectivity MRI networks arise from subject motion. NeuroImage. 2012; 59:2142–2154. [PubMed: 22019881]
38. Bradley MM, Codispoti M, Cuthbert BN, Lang PJ. Emotion and motivation I: defensive and appetitive reactions in picture processing. Emotion. 2001; 1:276–298. [PubMed: 12934687]
39. Codispoti M, Bradley MM, Lang PJ. Affective reactions to briefly presented pictures. Psychophysiology. 2001; 38:474–478. [PubMed: 11352135]
40. Milad MR, Quirk GJ. Neurons in medial prefrontal cortex signal memory for fear extinction. Nature. 2002; 420:70–74. [PubMed: 12422216]
41. Greicius MD, Flores BH, Menon V, Glover GH, Solvason HB, Kenna H, et al. Resting-state functional connectivity in major depression: abnormally increased contributions from subgenual cingulate cortex and thalamus. Biol Psychiatry. 2007; 62:429–437. [PubMed: 17210143]
42. Keedwell P, Drapier D, Surguladze S, Giampietro V, Brammer M, Phillips M. Neural markers of symptomatic improvement during antidepressant therapy in severe depression: subgenual cingulate and visual cortical responses to sad, but not happy, facial stimuli are correlated with changes in symptom score. J Psychopharmacol. 2009; 23:775–788. [PubMed: 18635699]
43. Matthews SC, Strigo IA, Simmons AN, Yang TT, Paulus MP. Decreased functional coupling of the amygdala and supragenual cingulate is related to increased depression in unmedicated individuals with current major depressive disorder. J Affect Disord. 2008; 111:13–20. [PubMed: 18603301]
44. Mayberg HS, Lozano AM, Voon V, McNeely HE, Seminowicz D, Hamani C, et al. Deep brain stimulation for treatment-resistant depression. Neuron. 2005; 45:651–660. [PubMed: 15748841]
45. Drevets WC, Bogers W, Raichle ME. Functional anatomical correlates of antidepressant drug treatment assessed using PET measures of regional glucose metabolism. Eur Neuropsychopharmacol. 2002; 12:527–544. [PubMed: 12468016]

46. Sheline YI, Barch DM, Donnelly JM, Ollinger JM, Snyder AZ, Mintun MA. Increased amygdala response to masked emotional faces in depressed subjects resolves with antidepressant treatment: an fMRI study. Biol Psychiatry. 2001; 50:651–658. [PubMed: 11704071]
47. Kross E, Davidson M, Weber J, Ochsner K. Coping with emotions past: the neural bases of regulating affect associated with negative autobiographical memories. Biol Psychiatry. 2009; 65:361–366. [PubMed: 19058792]
48. Mayberg HS, Liotti M, Brannan SK, McGinnis S, Mahurin RK, Jerabek PA, et al. Reciprocal limbic-cortical function and negative mood: converging PET findings in depression and normal sadness. Am J Psychiatry. 1999; 156:675–682. [PubMed: 10327898]
49. Zald DH, Mattson DL, Pardo JV. Brain activity in ventromedial prefrontal cortex correlates with individual differences in negative affect. Proc Natl Acad Sci U S A. 2002; 99:2450–2454. [PubMed: 11842195]
50. Blumer, D.; Benson, DF. Personality changes with frontal and temporal lesions. In: Benson, DF.; Blumer, D., editors. Psychiatric Aspects of Neurological Disease. Stratton; New York: 1975.
51. Koenigs M, Huey ED, Calamia M, Raymont V, Tranel D, Grafman J. Distinct regions of prefrontal cortex mediate resistance and vulnerability to depression. J Neurosci. 2008; 28:12341–12348. [PubMed: 19020027]
52. Koenigs M, Huey ED, Raymont V, Cheon B, Solomon J, Wassermann EM, et al. Focal brain damage protects against post-traumatic stress disorder in combat veterans. Nat Neurosci. 2008; 11:232–237. [PubMed: 18157125]
53. Damasio AR, Tranel D, Damasio H. Individuals with sociopathic behavior caused by frontal damage fail to respond autonomically to social stimuli. Behav Brain Res. 1990; 41:81–94. [PubMed: 2288668]
54. Bechara A, Damasio H, Tranel D, Damasio AR. Deciding advantageously before knowing the advantageous strategy. Science. 1997; 275:1293–1295. [PubMed: 9036851]
55. Camille N, Coricelli G, Sallet J, Pradat-Diehl P, Duhamel JR, Sirigu A. The involvement of the orbitofrontal cortex in the experience of regret. Science. 2004; 304:1167–1170. [PubMed: 15155951]
56. Qin P, Northoff G. How is our self related to midline regions and the default-mode network? Neuroimage. 2011; 57:1221–1233. [PubMed: 21609772]
57. Koenigs M, Grafman J. Posttraumatic stress disorder: the role of medial prefrontal cortex and amygdala. The Neuroscientist: a review journal bringing neurobiology, neurology and psychiatry. 2009; 15:540–548.
58. Barbas H, Saha S, Rempel-Clower N, Ghashghaei T. Serial pathways from primate prefrontal cortex to autonomic areas may influence emotional expression. BMC Neurosci. 2003; 4:25. [PubMed: 14536022]
59. Ghashghaei HT, Hilgetag CC, Barbas H. Sequence of information processing for emotions based on the anatomic dialogue between prefrontal cortex and amygdala. Neuroimage. 2007; 34:905–923. [PubMed: 17126037]
60. Ongur D, Price JL. The organization of networks within the orbital and medial prefrontal cortex of rats, monkeys and humans. Cereb Cortex. 2000; 10:206–219. [PubMed: 10731217]
61. Price JL, Amaral DG. An autoradiographic study of the projections of the central nucleus of the monkey amygdala. J Neurosci. 1981; 1:1242–1259. [PubMed: 6171630]
62. Neafsey EJ. Prefrontal cortical control of the autonomic nervous system: anatomical and physiological observations. Prog Brain Res. 1990; 85:147–165. discussion 165-146. [PubMed: 2094892]
63. Little JP, Carter AG. Synaptic mechanisms underlying strong reciprocal connectivity between the medial prefrontal cortex and basolateral amygdala. J Neurosci. 2013; 33:15333–15342. [PubMed: 24068800]
64. Sotres-Bayon F, Sierra-Mercado D, Pardilla-Delgado E, Quirk GJ. Gating of fear in prelimbic cortex by hippocampal and amygdala inputs. Neuron. 2012; 76:804–812. [PubMed: 23177964]
65. Baas D, Aleman A, Kahn RS. Lateralization of amygdala activation: a systematic review of functional neuroimaging studies. Brain Res Brain Res Rev. 2004; 45:96–103. [PubMed: 15145620]

66. Costafreda SG, Brammer MJ, David AS, Fu CH. Predictors of amygdala activation during the processing of emotional stimuli: a meta-analysis of 385 PET and fMRI studies. Brain Res Rev. 2008; 58:57–70. [PubMed: 18076995]

67. Wager TD, Phan KL, Liberzon I, Taylor SF. Valence, gender, and lateralization of functional brain anatomy in emotion: a meta-analysis of findings from neuroimaging. Neuroimage. 2003; 19:513–531. [PubMed: 12880784]

68. Sabatinelli D, Lang PJ, Bradley MM, Costa VD, Keil A. The timing of emotional discrimination in human amygdala and ventral visual cortex. J Neurosci. 2009; 29:14864–14868. [PubMed: 19940182]

69. Wilkinson, GS.; Robertson, GJ. WRAT4: Wide Range Achievement Test. Psychological Assessment Resources; Lutz, FL: 2006.

70. Watson D, Clark LA, Tellegen A. Development and validation of brief measures of positive and negative affect: the PANAS scales. Journal of personality and social psychology. 1988; 54:1063–1070. [PubMed: 3397865]

71. Beck, AT.; Steer, RA.; Brown, GK. Manual for the Beck Depression Inventory-II. Psychological Corporation; San Antonio, TX: 1996.

72. Spielberger, CD.; Gorsuch, RL.; Lushene, R.; Vagg, PR.; Jacobs, GA. Manual for the State-Trait Anxiety Inventory. Consulting Psychologists Press; Palo Alto, CA: 1983.

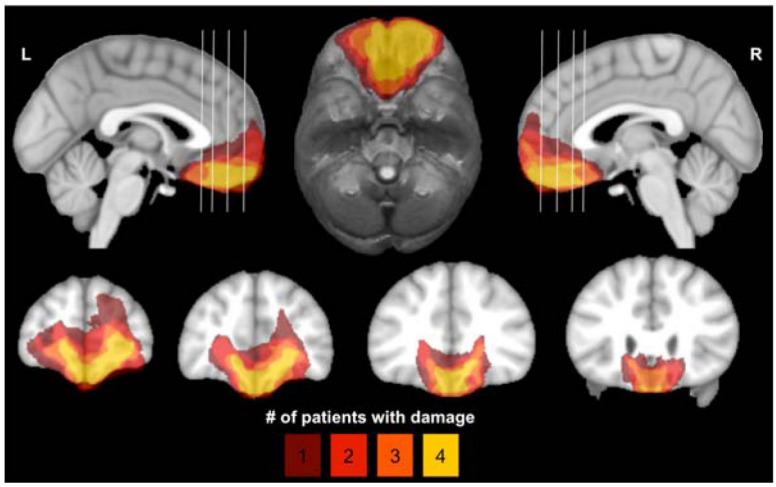

Figure 1.

Lesion overlap of vmPFC patients. Color indicates the number of overlapping lesions at each voxel. All vmPFC patients had damage to the medial one-third of the orbitofrontal cortex and the ventral one-third of medial surface of prefrontal cortex, bilaterally. This area includes Brodmann areas 11, 12, 24, 25, 32, and the medial portion of 10 below the level of the genu of the corpus callosum, as well as subjacent white matter.

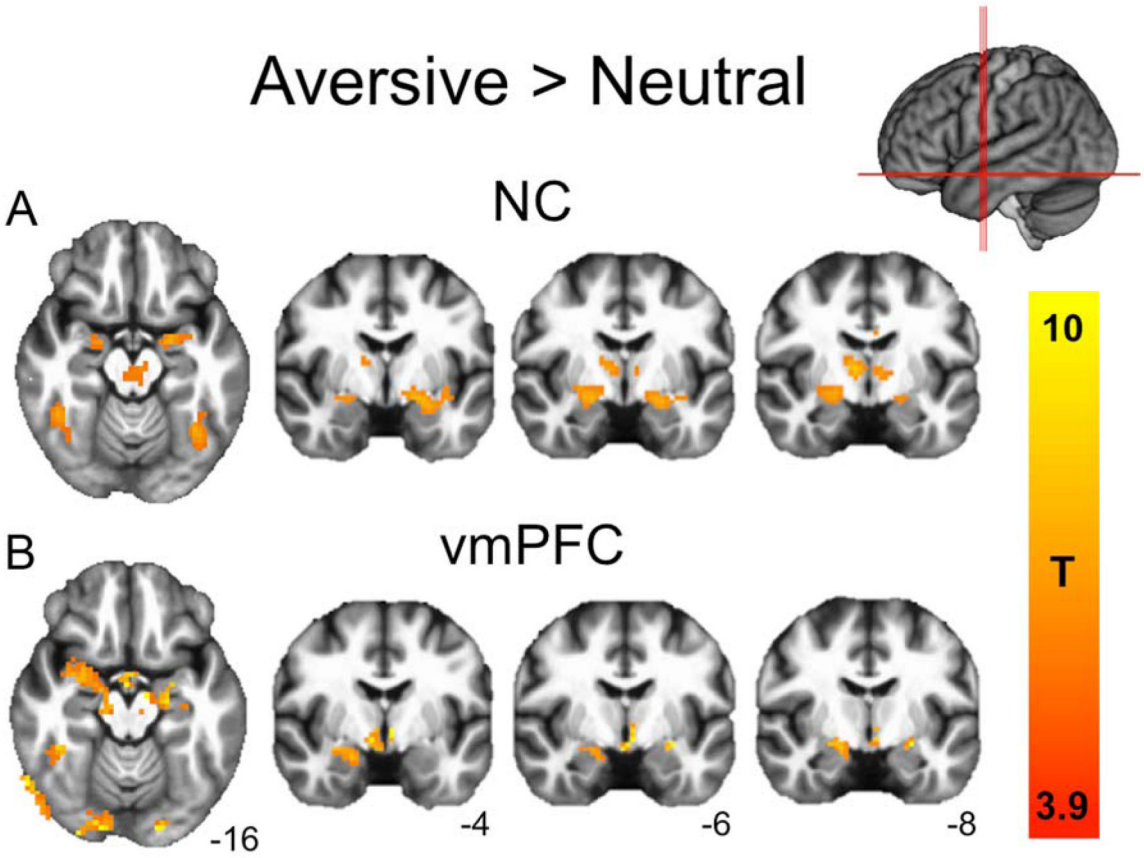

Figure 2.

Neural responses to aversive>neutral pictures. **(a)** NC subjects (P_{FWE}<0.05; FWE, family wise error). **(b)** vmPFC lesion patients (displayed at corrected NC threshold of T=3.9 for comparison). Both groups exhibited robust bilateral amygdala responses, as well as responses in visual cortex, lateral temporal cortex, thalamus, and cingulate gyrus (see Table 2 for full cluster list).

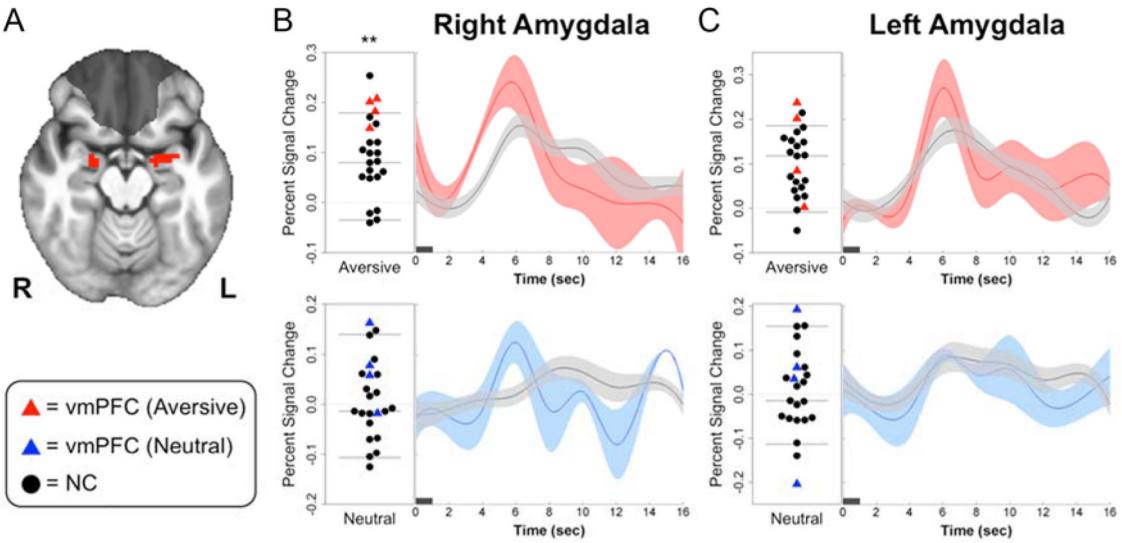

Figure 3.

Greater right amygdala responses to aversive pictures in vmPFC lesion patients. **(a)** Task-derived right and left amygdala ROIs (red) used to extract mean percent signal change (PSC) estimates for group comparisons. vmPFC lesion overlap shaded in gray for reference. **(b)** Left, plots of right amygdala PSC for individual NC (black circles) and vmPFC (red and blue triangles) subjects in response to aversive pictures (top) and neutral pictures (bottom). Horizontal lines represent the mean and 95% confidence intervals of PSC values in the NC group. Right, mean timeseries of right amygdala PSC in response to aversive and neutral pictures for vmPFC (red, blue) and NC (black) subjects (width of shaded area corresponds to ±1 s.e.m.). **(c)** Plot and mean timeseries of PSC extracted from the left amygdala ROI. Dark horizontal bars on timeseries plots indicate picture duration (1 s). ***P*<0.01

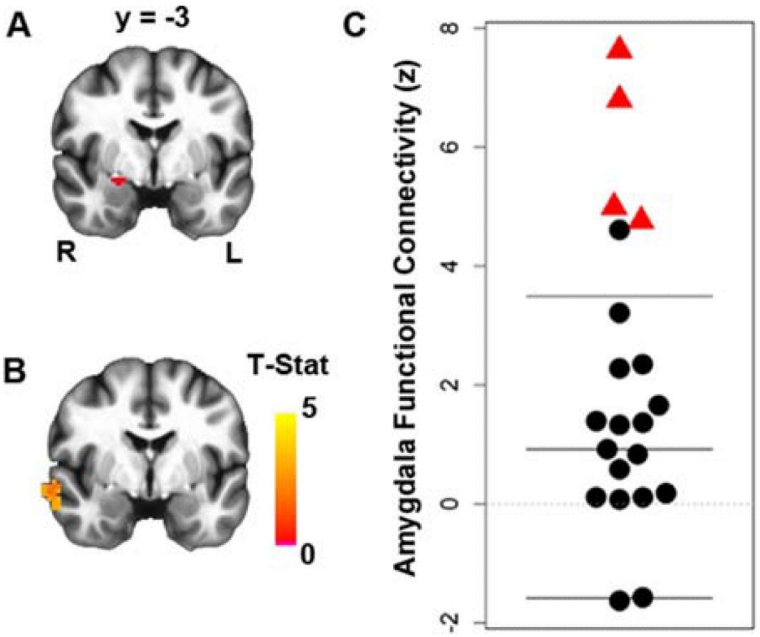

Figure 4.

Greater right amygdala rest-state functional connectivity in vmPFC lesion patients. **(a)** Right amygdala seed region (red). **(b)** Group difference map at corrected $P_{FWE}<0.05$, showing greater right amygdala connectivity with a cluster in the ipsilateral anterior temporal lobe in the vmPFC lesion group (see Fig. S4 for average amygdala connectivity maps from each group). **(c)** Plot showing distribution of connectivity values (z-scores) in the significant cluster.

Table 1

Subject characteristics

	Age	Sex	Edu	IQ	Pos Aff	Neg Aff	BDI-II	STAI-T
vmPFC (n=4)	58.5 (6.2)	3 M 1 F	15.5 (4.1)	103.8 (12.4)	36 (8.4)	17.0 (8.7)	7.0 (3.2)	34.3 (9.5)
NC (n=19)	51.7 (9.9)	11 M 8 F	17.7 (3.5)	110.9 (7.2)	37.8 (4.9)	13.0 (2.4)	4.0 (3.3)	31.6 (6.0)
NC age 50+ (n=10)	59.8 (4.7)	8 M 2 F	16.8 (2.3)	113.1 (7.2)	39.2 (5.4)	12.6 (2.7)	3.7 (2.9)	29.6 (5.0)
P (vmPFC vs NC)	0.16	0.63	0.51	0.25	0.56	0.73	0.11	0.44
P (vmPFC vs NC age 50+)	0.95	0.99	0.64	0.14	0.54	0.64	0.13	0.28

Means are presented with standard deviations in parentheses. Edu, years of education; IQ, intelligence quotient estimated by the Wide Range Achievement Test 4, Blue Reading subtest (69); Pos/Neg Aff, scores from the Positive and Negative Affect Schedule (PANAS) (70); BDI-II, Beck Depression Inventory-II (71) ; STAI-T, trait version of the Spielberger State Trait Anxiety Inventory (72).

Table 2

Cluster maxima for regions with statistically significant increased BOLD signal for aversive pictures relative to neutral pictures

NC group								vmPFC group	
				Peak voxel					
Brain region	BA	Clust size	p (FWE)	t	x	y	z	t	p
R ITG	37	684	<0.0001	12.50	47	−68	−3	3.47	0.040
Thal		337	<0.0001	11.16	−1	−27	−4	1.99	0.141
L MTG	37	597	<0.0001	8.84	−52	−69	6	3.07	0.055
R Lingual	17	283	<0.0001	7.00	17	−90	−3	1.36	0.267
L Amyg	28	72	<0.005	6.49	−19	−3	−12	2.23	0.112
R Amyg	28	39	<0.05	6.03	20	−6	−12	3.38	0.043
R Precun	31	64	<0.005	6.00	5	−48	33	−0.85	0.458
L MFG	9	68	<0.005	5.23	−7	51	27	0.90	0.434
L ACC	24/32	72	<0.005	4.86	−1	6	39	0.87	0.448
L PCC	23	62	<0.005	4.58	−7	−24	27	−1.55	0.219

Clusters ordered by T score, for the aversive>neutral contrast in the NC group. Corrected p thresholds indicate minimum FWE-corrected p-value for each cluster. Uncorrected p values for the vmPFC group are derived from a voxelwise paired t-test in the vmPFC group, estimated at the peak coordinates for the NC group. R, right; L, left; ITG, inferior temporal gyrus; Thal, thalamus; MTG, middle temporal gyrus; Lingual, lingual gyrus; Amyg, amygdala; Precun, precuneus; MFG, medial frontal gyrus; ACC, anterior cingulate cortex; PCC, posterior cingulate cortex.

Table 3

Group differences in percent signal change to aversive and neutral pictures in functional and anatomical ROIs

	Region of Interest				Aversive pictures				Neutral pictures			
Brain Region	Size	Center of Mass			NC mean (SD)	vmPFC mean (SD)	W	*P*	NC mean (SD)	vmPFC mean (SD)	W	*P*
		X	Y	Z								
R Amyg (Func ROI)	39	23	−6.3	−9.6	0.08 (0.07)	0.18 (0.03)	6	**0.006**	0.00 (0.08)	0.07 (0.07)	20	0.162
R Amyg (Anat ROI)	18	25	−3.8	−16	0.09 (0.08)	0.19 (0.07)	13	**0.044**	0.02 (0.08)	0.05 (0.12)	31	0.611
R Amyg (CeA ROI)	6	23	−7.5	−15	0.09 (0.08)	0.18 (0.06)	13	**0.044**	0.00 (0.09)	0.06 (0.09)	23	0.25
L Amyg (Func ROI)	72	−25	−2.7	−12	0.10 (0.07)	0.13 (0.11)	28	0.456	0.01 (0.08)	0.02 (0.17)	31	0.611
L Amyg (Anat ROI)	29	−23	−4.2	−17	0.10 (0.08)	0.16 (0.11)	24	0.286	0.02 (0.09)	0.03 (0.14)	32	0.667
L Amyg (CeA ROI)	6	−22	−7.5	−15	0.12 (0.09)	0.19 (0.11)	24	0.286	0.01 (0.09)	0.01 (0.19)	31	0.612
R ITG	684	46	−68	4	0.34 (0.13)	0.42 (0.11)	23	0.25	0.22 (0.11)	0.31 (0.07)	20	0.162
L MTG	597	−43	−71	6.6	0.30 (0.12)	0.35 (0.07)	26	0.366	0.20 (0.10)	0.25 (0.02)	22	0.218
Thal	337	0.9	−20	−2.2	0.14 (0.08)	0.18 (0.02)	24	0.286	0.06 (0.08)	0.11 (0.07)	23	0.25
R Lingual	283	6.7	−87	1.3	0.48 (0.18)	0.50 (0.14)	31	0.611	0.38 (0.14)	0.44 (0.08)	24	0.286
L ACC	72	−1.5	15	32	0.10 (0.06)	0.10 (0.06)	40	0.907	0.02 (0.09)	0.07 (0.06)	23	0.25
L MFG	68	−8.5	51	26	0.03 (0.09)	0.01 (0.12)	41	0.845	−0.08 (0.07)	−0.04 (0.06)	26	0.366
R Precun	64	0.1	−50	31	−0.01 (0.06)	−0.02 (0.04)	45	0.611	−0.06 (0.07)	0.01 (0.03)	17	0.097
L PCC	62	−1.3	−18	33	0.05 (0.05)	−0.03 (0.12)	56	0.162	−0.02 (0.06)	0.02 (0.08)	27	0.409

p-values for significant group differences are in bold. Cluster size in number of voxels (3×3×3 mm^3). Center of mass coordinates for each ROI presented in MNI space. Func ROI, functionally-defined ROI; Anat ROI, anatomically-defined ROI.